Journal of Histochemistry & Cytochemistry 2016, Vol. 64(9) 530–545

DOI: 10.1369/0022155416656842
jhc.sagepub.com
SAGE

Effects of Oxaliplatin Treatment on the Enteric Glial Cells and Neurons in the Mouse Ileum

Ainsley M. Robinson, Vanesa Stojanovska, Ahmed A. Rahman, Rachel M. McQuade, Paul V. Senior, and Kulmira Nurgali

Centre for Chronic Diseases, College of Health and Biomedicine, Victoria University, Melbourne, Australia (AMR, VS, AAR, RMM, KN); Department of Surgery, University of Melbourne, Melbourne, Australia; and Western Centre for Health Research & Education, Western Health, Sunshine Hospital, St Albans, Australia (PVS)

Summary

Oxaliplatin, currently used for treatment of colorectal and other cancers, causes severe gastrointestinal side effects, including nausea, vomiting, diarrhea, and constipation that are attributed to mucosal damage. However, delayed onset and long-term persistence of these side effects suggest that damage to the enteric nervous system (ENS) regulating physiological function of the gastrointestinal tract may also occur. The ENS comprises myenteric and submucosal neurons and enteric glial cells (EGCs). This study aimed to investigate the effects of oxaliplatin treatment on enteric neurons and EGCs within the mouse ileum. BALB/c mice received repeated intraperitoneal injections of oxaliplatin (3 mg/kg, 3 injections/week). Tissues were collected 3, 7, 14, and 21 days from the commencement of treatment. Decreases in glial fibrillary acidic protein–immunoreactive (IR) EGCs and protein gene product 9.5/β-Tubulin III-IR neurons as well as increase in s100β-IR EGCs after chronic oxaliplatin administration were observed in both the myenteric and submucosal plexi. Changes in EGCs were further observed in cross-sections of the ileum at day 14 and confirmed by Western blotting. Alterations in EGCs correlated with loss of myenteric and submucosal neurons in the ileum from oxaliplatin-treated mice. These changes to the ENS may contribute to the mechanisms underlying gastrointestinal side effects associated with oxaliplatin treatment. (J Histochem Cytochem 64:530–545, 2016)

Keywords

chemotherapy, enteric glial cells, GFAP, myenteric and submucosal neurons, oxaliplatin, s100β

Introduction

Platinum-based chemotherapeutic agents, including cisplatin, carboplatin, and oxaliplatin, are commonly used for the treatment of colorectal cancer and are typically associated with increased patient response and survival rates.[1–3] Oxaliplatin is the only platinum analogue that demonstrates single-agent activity against colorectal cancer.[2,4] Although oxaliplatin has proven to be highly effective, its use is associated with severe sensory neuropathy and gastrointestinal side effects, such as diarrhea, constipation, nausea, and vomiting.[5–8]

Both gastrointestinal side effects and oxaliplatin-induced sensory neuropathy are recognized as dose-limiting complications of oxaliplatin treatment leading to a discontinuation of chemotherapy and limiting the effectiveness of anticancer treatment.[5,9,10] Because most chemotherapeutic agents target the DNA synthesis mechanism, it is generally considered that gastrointestinal side effects of anticancer chemotherapies are due to the damage to the intestinal mucosa where rapid cell turnover

Received for publication January 27, 2016; accepted June 6, 2016.

Corresponding Author:
Kulmira Nurgali, Western Centre for Health Research & Education, Sunshine Hospital, 176 Furlong Road, St Albans, VIC 3021, Australia.
Email: kulmira.nurgali@vu.edu.au

occurs.[6] However, platinum-based chemotherapeutic agents can damage both mucosa and amitotic cells, such as enteric neurons innervating the gastrointestinal tract.[11,12]

It has been well established that the enteric nervous system (ENS), consisting of enteric neurons and enteric glial cells (EGCs), is responsible for physiological regulation of gastrointestinal functions.[13] EGCs have been previously considered as counterparts to astrocytes of the central nervous system (CNS) acting as supportive cells for enteric neurons. However, it is now known that in addition to sustaining the structural and functional integrity of enteric neurons,[14–19] EGCs are directly involved in gastrointestinal motility, neurotransmission, immune functions, and maintaining intestinal epithelial integrity.[16,20–24] Furthermore, an enteric neuroglial interaction has been established through an association between ENS damage and the destruction of EGCs.[22,25,26] EGCs can proliferate and be activated in response to injury and inflammation.[27,28]

Previous studies have shown that in the CNS, astrocytes are sensitive to the platinum drug toxicity[29] and contribute to the development and persistence of chronic pain.[30,31] Glial cell inhibition in the CNS reduces oxaliplatin-induced pain.[32] Loss of myenteric neurons was observed in the stomach and colon of cisplatin-treated rats and mice[12,33] and in the colon of oxaliplatin-treated mice,[34] which was associated with changes in gastric contractile activity and colonic dysmotility. However, very little is known about the actions of platinum-based chemotherapeutic agents on the ENS. In this study, we investigated the effects of repeated in vivo oxaliplatin administration on EGCs and enteric neurons in the mouse ileum.

Materials and Methods

Animals

Male BALB/c mice aged 6–8 weeks (18–25 g, *n*=32) were obtained from the Animal Resources Centre (Perth, Australia). All mice had free access to food and water and were housed in a temperature-controlled environment with a 12-hr light/dark cycle. The acclimatization period was at least 3 days before commencement of in vivo intraperitoneal injections. All procedures used throughout this study were conducted according to the guidelines of the National Health and Medical Research Council (NHMRC) Australian Code of Practice for the Care and Use of Animals for Scientific Purposes and were approved by the Victoria University Animal Experimentation Ethics Committee.

In Vivo Intraperitoneal Injections

Mice received either sham or oxaliplatin in vivo intraperitoneal injections three times a week via a 26G needle. Oxaliplatin (Tocris Bioscience, Bristol, UK) was dissolved in sterile water to make 10^{-2} mM stock solutions and stored at –20C. Before use, the stock was diluted further into 10^{-3} mM solutions for intraperitoneal injections. The dose of oxaliplatin (3 mg/kg) used in this study was calculated to be equivalent to the standard human dose per body surface area.[35,36] Sham treatments comprised intraperitoneal injection of sterile water (maximum volume 200 µL). Mice were weighed daily and monitored for signs of pica (ingestion of nonnutritive substances, for example, bedding materials), diarrhea, and constipation during treatment regimes. Mice were euthanized by cervical dislocation 3, 7, 14, or 21 days after the first injection was administered. Ileum specimens were collected for immunohistochemical and Western blot analyses.

Tissue Preparation

Following dissection, tissues were placed in oxygenated phosphate-buffered saline (PBS; 0.1 M, pH = 7.2) containing an L-type Ca^{2+} channel blocker, nicardipine (3 µm; Sigma-Aldrich, Sydney, Australia) to inhibit smooth muscle contraction. Samples were cut open along the mesenteric border and cleared of their contents. Tissues were then processed in three different ways: (1) whole mount longitudinal muscle-myenteric plexus (LMMP) preparations, (2) submucosal plexus (SMP) preparations, and (3) cross-sections.

LMMP and SMP Preparations. Ileum specimens were pinned flat and stretched to maximal capacity without tearing in a Sylgard-lined Petri dish. For SMP preparations, the longitudinal muscle, myenteric plexus, and circular muscle layers were removed before fixation. Tissues were fixed overnight at 4C in Zamboni's fixative (2% formaldehyde and 0.2% picric acid) and subsequently washed for 3 × 10 min in dimethyl sulfoxide (DMSO; Sigma-Aldrich) followed by 3 × 10 min in 0.1 M PBS to remove fixative. In this study, Zamboni's fixative was chosen for tissue fixation to minimize neural tissue autofluorescence. For LMMP preparations, the ileum specimens were dissected to expose the myenteric plexus by removing the mucosa, submucosa, and circular muscle layers before immunohistochemistry (IHC).

Cross-Sections. Tissues for cross-sections were pinned with the mucosal side up in a Sylgard-lined Petri dish, without stretching. Tissues for cryostat cross-sections were fixed as described above. After fixation tissues were

Table 1. Primary and Secondary Antisera Used in This Study.

Primary Antiserum	Host Species	Dilution	Source	Application in This Study
Anti-GFAP	Goat	1:1000	Sigma-Aldrich	Myenteric plexus Submucosal plexus Cross-sections Western blot
Anti-s100β	Rabbit	1:500	Abcam (Melbourne, Australia)	Myenteric plexus Submucosal plexus Cross-sections
Anti-s100β	Mouse	1:1000	Abcam	Western blot
Anti-PGP9.5	Chicken	1:500	Abcam	Myenteric plexus
Anti-β-Tubulin class III	Chicken	1:1000	Abcam	Submucosal plexus Western blot
Antismooth muscle actin	Rabbit	1:1000	Abcam	Western blot
Secondary Antiserum	**Host Species**	**Dilution**	**Source**	**Application in This Study**
FITC 488	Donkey anti-goat	1:200	Jackson Immunoresearch Laboratories (West Grove, PA)	Myenteric plexus Submucosal plexus Cross-sections
Alexa Fluor 594	Donkey anti-rabbit	1:200	Jackson Immunoresearch Laboratories	Myenteric plexus Cross-sections
FITC 488	Donkey anti-rabbit	1:200	Jackson Immunoresearch Laboratories	Myenteric plexus
Alexa Fluor 647	Donkey anti-rabbit	1:200	Jackson Immunoresearch Laboratories	Submucosal plexus
Alexa Fluor 594	Donkey anti-chicken	1:200	Jackson Immunoresearch Laboratories	Submucosal plexus
HRP-conjugated	Anti-goat	1:2000	Abcam	Western blot
HRP-conjugated	Anti-mouse	1:2000	Abcam	Western blot
HRP-conjugated	Anti-chicken	1:2000	Abcam	Western blot
HRP-conjugated	Anti-rabbit	1:2000	Abcam	Western blot

Abbreviations: GFAP, glial fibrillary acidic protein; PGP9.5, protein gene product 9.5; FITC, fluorescein isothiocyanate; HRP, horse-radish peroxidase.

stored in 50:50 optimum cutting temperature (OCT) compound (Tissue-Tek, Torrance, CA) and sucrose solution for 24 hr at 4C and subsequently frozen in liquid nitrogen-cooled isopentane and OCT compound. Samples were stored at –80C until they were cryo-sectioned (30 µm) onto glass slides for IHC. Tissues for histology cross-sections were fixed in 10% buffered formalin overnight at 4C and stored in 70% ethanol until embedding.

IHC

IHC was performed on whole mount LMMP preparations, submucosal preparations, and cross-sections. After 1-hr incubation in 10% normal donkey serum (NDS; Merck Millipore, Bayswater, Australia) diluted in 0.1 M PBS-0.1% Triton X-100 at room temperature, the specimens were washed with 0.1 M PBS-0.1% Triton X-100 (2 × 5 min) and incubated with primary antibodies (Table 1) diluted in 2% NDS and 0.1 M PBS-0.1% Triton X-100 overnight at room temperature. Tissues were then washed in 0.1 M PBS-0.1% Triton X-100 (2 × 5 min) before incubation with secondary antibodies (Table 1; diluted in 2% NDS and 0.1 M PBS-0.1% Triton X-100) for 2 hr at room temperature. Following 3 × 10 min washes in 0.1 M PBS-0.1% Triton X-100, LMMP and SMP samples were mounted on glass slides with fluorescent mounting medium (DAKO, Sydney, Australia). Negative control experiments were performed for all antibodies used in this study.

Histology

After paraffin embedding, tissues for histology were sectioned at 5 µm, deparaffinized, cleared, and rehydrated in graded ethanol concentrations. For standard hematoxylin and eosin (H&E) staining, sections were immersed in xylene (3 × 4 min), 100% ethanol (3 min), 90% ethanol (2 min), 70% ethanol (2 min), rinsed in tap water, hematoxylin (4 min), rinsed in tap water, Scott's tap water (1 min), eosin (6 min), rinsed in tap water, 100% ethanol (2 × 1 min), xylene (2 × 3 min), and mounted with distrene plasticizer xylene.

Imaging

Confocal microscopy was performed on an Eclipse Ti confocal laser scanning system (Nikon, Lidcombe,

Australia). Fluorophores were visualized using a 488-nm excitation filter for fluorescein isothiocyanate and a 559-nm excitation filter for Alexa 594. Z-series images were acquired at a nominal thickness of 0.5 µm (512 × 512 pixels) with 20× (dry, 0.75) or 40× (oil immersion, 1.3) lenses. H&E-stained ileum sections were visualized using an Olympus BX53 microscope (Olympus, Notting Hill, Australia), and images were captured with CellSense software.

Quantitative Analysis of Immunohistochemical and Histological Data

The immunoreactivity of protein gene product 9.5 (PGP9.5) neurons in the myenteric plexus and of β-Tubulin (III) neurons in the SMP and changes to glial fibrillary acidic protein (GFAP)–immunoreactive (IR) and s100β-IR EGC populations following oxaliplatin treatment were assessed by analyzing the density of labeling per area (eight images per preparation at 20× magnification [total area = 2 mm^2]). All images were captured at identical acquisition exposure-time conditions, calibrated to standardized minimum baseline fluorescence, and converted to binary, and changes in fluorescence from baseline were measured using Image J software (National Institute of Health, Bethesda, MD). All images were analyzed blindly. In LMMP preparations, the number of colocalizing GFAP/s100β-IR EGCs was counted per ganglion in images at 40× magnification and averaged per 10 ganglia in each preparation. Overall histological scores (out of 15) were developed from the following parameters: aberrant crypt architecture (score range = 0–3), changes to crypt length (0–3), crypt abscesses (0–3), leukocyte infiltration (0–3), and epithelial damage and ulceration (0–3; average of eight areas of 500 μm^2 per animal). Histological scoring was performed blindly.

Western Blotting

Western blotting experiments were performed on the smooth muscle and enteric ganglia layers after the mucosal layer of the ileum was microdissected and discarded. Tissue samples were then homogenized for 30 sec and centrifuged at 12,000 rpm for 20 min at 4C. Protein levels were quantified using the bicinchoninic acid assay (Thermo Fisher Scientific, Scoresby, Australia) according to manufacturers' instructions, and absorbance was read at 526 nm by the Varioskan Flash Multimode Reader using SkanIt software v2.4.3 (Thermo Fisher Scientific). Protein samples (15 µg/lane) were prepared and separated by sodium dodecyl sulfate-polyacrylamide gel electrophoresis using 4% to 20% StainFree gels (Bio-Rad, Gladesville, Australia). Precision Plus Protein Prestained Standard (Bio-Rad; 5 µL) was loaded as the molecular weight marker. Proteins were transferred using a TransBlot Turbo (Bio-Rad) to polyvinylidene difluoride (PVDF) membranes, and total protein transferred was imaged (Gel Doc EZ and Image Lab v5 software [Bio-Rad]). PVDF membranes with transferred proteins were blocked in 0.1 M PBS containing 5% nonfat dry milk powder (w/v) for 1 hr at room temperature. Membranes were washed in 0.1 M PBS and 10% Tween 20 before incubating with primary antibodies (Table 1) diluted in 0.1 M PBS, 10% Tween 20, and 5% nonfat dry milk powder overnight at 4C. Membranes were then washed and incubated with horse-radish peroxidase–conjugated secondary antibodies (Table 1) for 1 hr at room temperature. Membranes were then subjected to chemiluminescence reagents (Bio-Rad) for 3 min and imaged using the VersaDoc MP4000 (Bio-Rad) system. Image Lab v5 was used for analysis to obtain protein expression values in arbitrary units.[37] Smooth muscle actin was used as the loading control.

Statistical Analysis

Data were presented as mean ± standard error of the mean, if not specified otherwise. Statistical differences were determined by one-way ANOVA with Tukey–Kramer or Bonferroni post hoc tests for multiple group comparisons or Student's two-tailed *t*-test using Prism v5.0 (GraphPad Software). Data were considered statistically significant when $p<0.05$.

Results

Effects of Oxaliplatin Treatment on Weight Gain and Gross Morphology of the Ileum

In this study, symptoms of gastrointestinal side effects were observed in mice soon after the first injection of oxaliplatin, for example, pica behavior, as well as succeeding repeated oxaliplatin administrations, for example, constipation.

To demonstrate the systemic impact of the oxaliplatin treatments, mice were weighed daily during the treatment regime ($n=4$ animals/group/time point; Fig. 1A). Sham-treated mice consistently gained weight over 21 days (3 days: 104.3 ± 0.2%, 7 days: 105.3 ± 0.1%, 14 days: 111.7 ± 1.2%, 21 days: 115.3 ± 2.5%). In contrast, oxaliplatin-treated mice did not demonstrate any differences in weight gain at 3 (101.0 ± 1.0%) and 7 (102.4 ± 1.0%) days after the initial treatment when compared with sham-treated mice. At 14 and 21 days of repeated oxaliplatin injections, mice had significantly lower weight compared with sham-treated mice ($p<0.05$ for both, 14 days: 102.1 ± 2.1%, 21 days: 105.5 ± 1.3%).

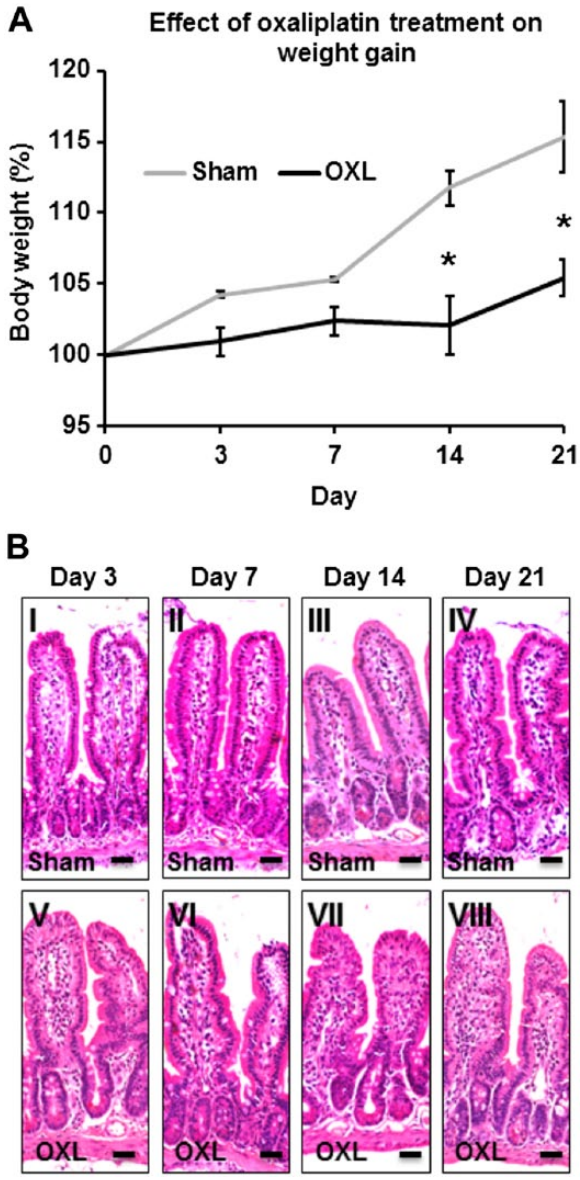

Figure 1. The effect of in vivo oxaliplatin treatment on weight gain and gross morphology of the ileum. (A) Body weight of mice recorded at 3, 7, 14, and 21 days post initial oxaliplatin or sham treatments. n=4 mice/group/time point. *p<0.05. (B) Gross morphology of the ileum assessed in hematoxylin and eosin (H&E)–stained cross-sections from oxaliplatin- and sham-treated mice at 3, 7, 14, and 21 days after the first injection. Scale bars = 25 μm, n=3 mice/group/time point. Abbreviation: OXL = oxaliplatin.

No obvious macroscopic abnormalities were observed in the ileum at the time points we studied. Gross morphological assessment of H&E-stained sections enabled microscopic evaluation of changes to the ileal architecture following oxaliplatin treatment(s) (n=3 animals/group/time point; Fig. 1B). H&E-stained ileum cross-sections from sham-treated mice displayed normal villi and structural arrangements of goblet cells and crypts, a continuous epithelial cell lining and distinct muscular and mucosal layers at 3, 7, 14, and 21 days post initial treatment (histological scores = 0–1, for all time points; Fig. 1B, I–IV). No differences were observed in H&E-stained ileum sections from oxaliplatin-treated mice after short- and long-term oxaliplatin treatments (histological scores = 0–1, for all time points; Fig. 1B, V–VIII) when compared with sham-treated mice.

Effects of Oxaliplatin Treatment on the Myenteric GFAP-IR EGCs

Immunohistochemical labeling of both oxaliplatin-treated and sham-treated ileum tissues revealed GFAP-IR EGCs within the myenteric plexus (Fig. 2). Quantification of GFAP immunoreactivity was completed by measuring the density of labeling per 2 mm^2 area. There were no changes in the density of GFAP-IR labeling in tissues from oxaliplatin-treated mice at days 3 (3.4 ± 0.3%) and 7 (3.1 ± 0.2%) when compared with tissues from the sham-treated mice (day 3: 3.5 ± 0.3%, day 7: 3.5 ± 0.2%; n=3 animals/group/time point; Figs. 2A–D^{I}, I). Long-term oxaliplatin administration induced a decrease in the density of GFAP-IR EGCs in tissues from oxaliplatin-treated mice when compared with tissues from sham-treated mice (Figs. 2E–H, I). After 14 days of oxaliplatin treatment, the density of GFAP-IR in the mouse ileum was considerably reduced (oxaliplatin: 2.5 ± 0.1%, sham: 3.6 ± 0.3%, p<0.05; n=3 mice/group/time point; Fig. 2I). Quantification of the density of GFAP-IR labeling at 21 days after the commencement of oxaliplatin treatment demonstrated no further loss of GFAP-IR in the oxaliplatin-treated group (2.4 ± 0.1%) compared with the sham-treated group (3.5 ± 0.2%, p<0.05; n=3 mice/group/time point; Fig. 2I).

Effects of Oxaliplatin Treatment on the Myenteric s100β-IR EGCs

There were no changes to the density of s100β-IR EGCs at days 3 and 7 in the oxaliplatin-treated group (day 3: 5.3 ± 0.4%, day 7: 5.1 ± 0.2%) when compared with sham-treated animals (day 3: 5.6 ± 0.1%, day 7: 5.8 ± 0.2%; n=3 mice/group/time point; Figs. 3A–D^{I}, I). The density of s100β-IR in the myenteric plexus of the ileum increased in tissues from oxaliplatin-treated mice (6.6 ± 0.2%) after 14 days when compared with tissues from sham-treated mice (5.7 ± 0.2%, p<0.01; n=3 mice/group/time point; Figs. 3E and F^{I}, I). At 21 days after the commencement of treatment, the density of s100β-IR EGCs in oxaliplatin tissues (6.5 ±

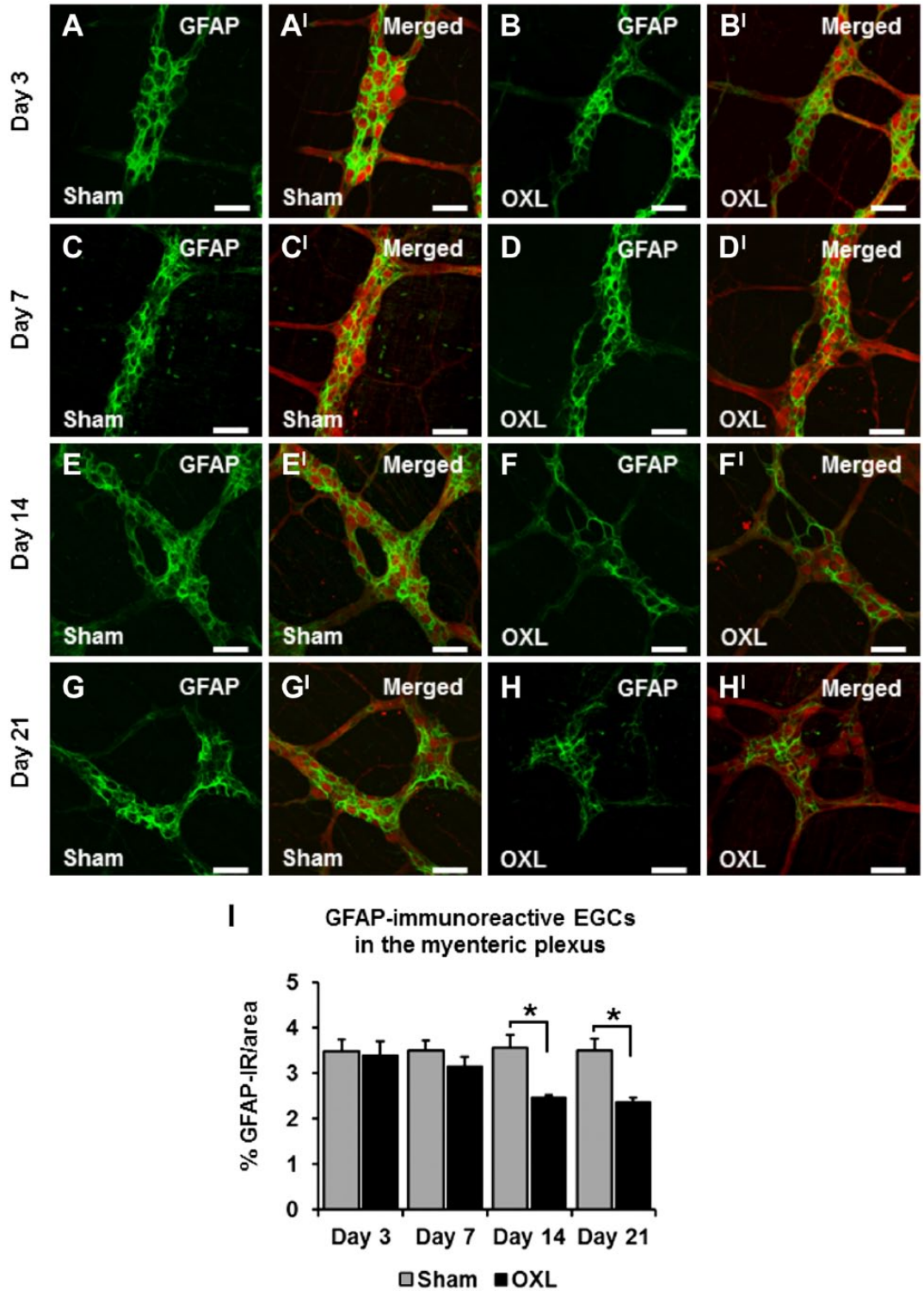

Figure 2. The effect of in vivo oxaliplatin treatment on glial fibrillary acidic protein–immunoreactive (GFAP-IR) enteric glial cells (EGCs) in the myenteric plexus. GFAP immunoreactivity in longitudinal muscle-myenteric plexus (LMMP) ileum preparations 3, 7, 14, and 21 days after commencement of oxaliplatin treatment (A–H). Merged images depicting GFAP-IR EGCs surrounding protein gene product 9.5-IR (PGP9.5-IR) myenteric neurons (A^{I}–H^{I}). Scale bars = 50 µm. Quantitative analyses of the density of GFAP immunoreactivity per 2 mm^2 area (I). *n*=3 mice/group/time point. Abbreviation: OXL = oxaliplatin. **p*<0.05.

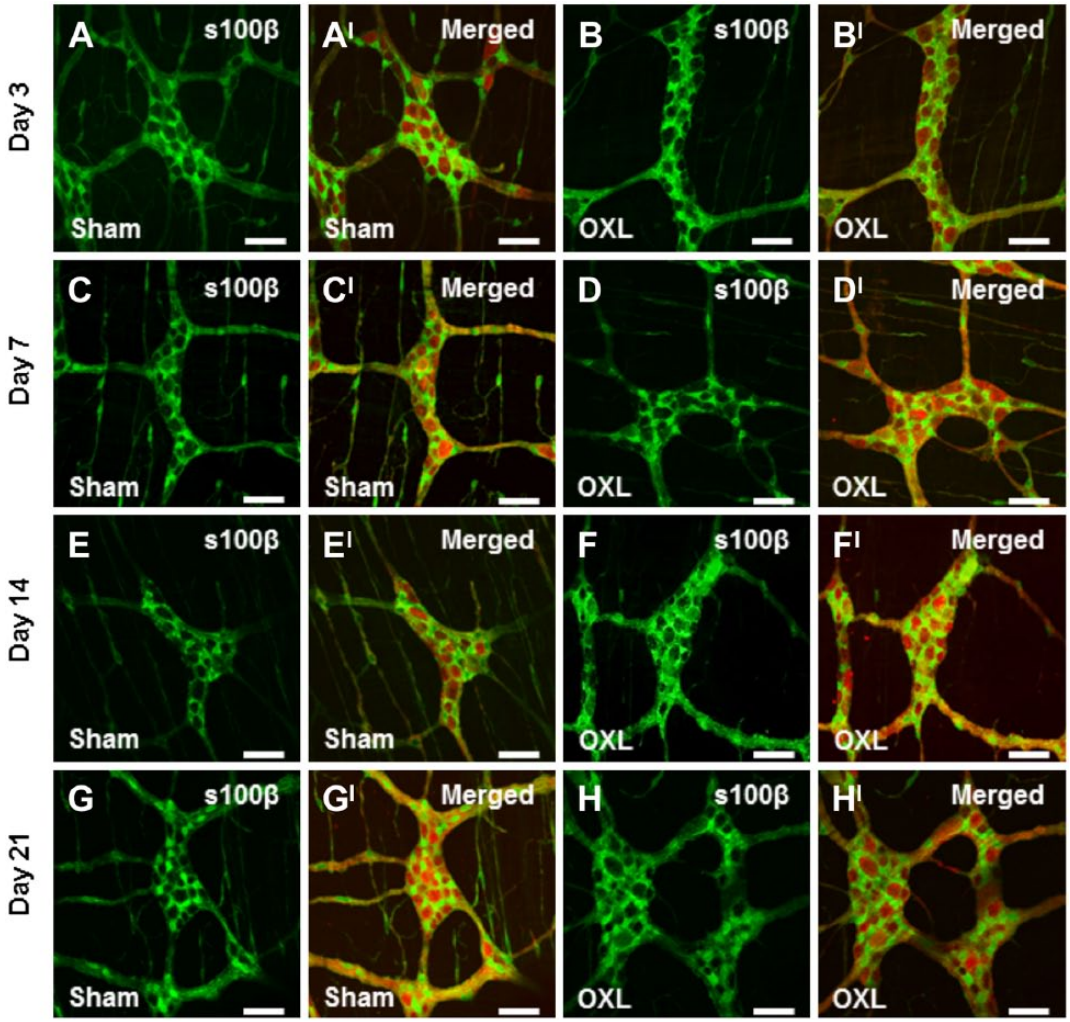

Figure 3. The effect of in vivo oxaliplatin treatment on s100β-immunoreactive (IR) enteric glial cells (EGCs) in the myenteric plexus. s100β immunoreactivity in longitudinal muscle-myenteric plexus (LMMP) ileum preparations 3, 7, 14, and 21 days after commencement of oxaliplatin treatment (A–H). Merged images depicting s100β-IR EGCs surrounding protein gene product 9.5-IR (PGP9.5-IR) myenteric neurons (A^{I}–H^{I}). Scale bars = 50 μm. Quantitative analysis measuring the density of s100β immunoreactivity per 2 mm^2 area (I). n=3 mice/group/time point. Abbreviation: OXL = oxaliplatin. **p<0.01.

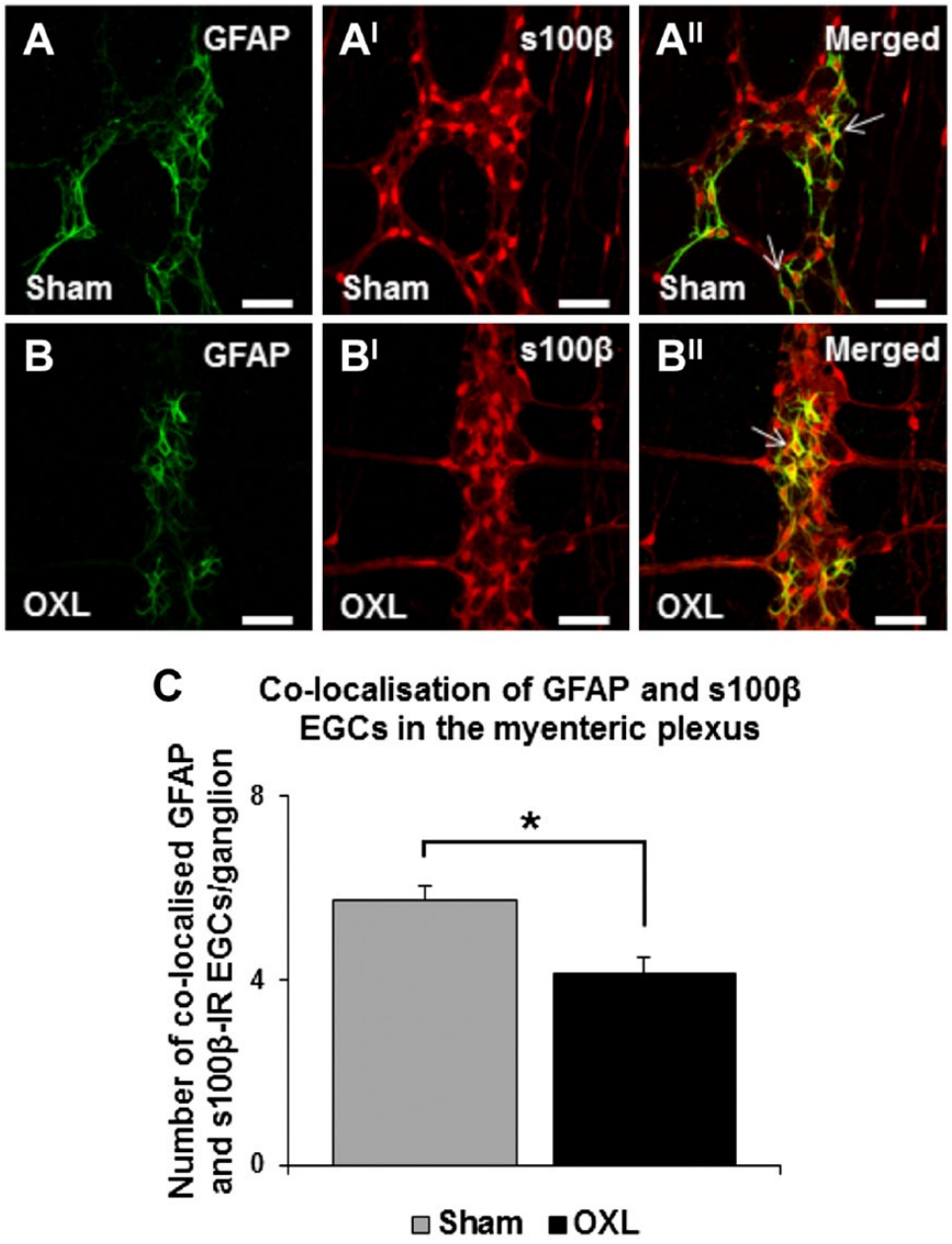

Figure 4. The effect of in vivo oxaliplatin treatment on glial fibrillary acidic protein (GFAP) and s100β-colocalizing enteric glial cells (EGCs) in the myenteric plexus. GFAP (A–B) and s100β (A^{I}–B^{I}) immunoreactivity in longitudinal muscle-myenteric plexus (LMMP) ileum preparations 14 days after commencement of sham or oxaliplatin treatment. Merged images depicting GFAP and s100β-colocalizing EGCs in the myenteric plexus (A^{II}–B^{II}). Scale bars = 50 μm. Quantitative analysis of the number of colocalizing EGCs per ganglion (C). *n*=3 mice/group/time point. Abbreviation: OXL = oxaliplatin. *p<0.05.

0.1%) remained consistently elevated in comparison with sham-treated mice (5.6 ± 0.1%, p<0.01; *n*=3 mice/group/time point; Figs. 3G and H^{I}, I).

The effects of oxaliplatin treatment on colocalization of myenteric GFAP and s100β-IR EGCs was assessed in the LMMP preparations of the ileum 14 days after the commencement of oxaliplatin treatment (Figs. 4A and B^{II}). EGCs colabeled with GFAP and s100β antibodies were counted and averaged per 10 ganglia. An average of 5.8 ± 0.3 GFAP/s100β-IR EGCs per ganglion were observed in sham-treated mice. Oxaliplatin treatment significantly reduced the number of GFAP/s100β-IR colocalizing EGCs (4.2 ± 0.3 per ganglion, p<0.05; Fig. 4C).

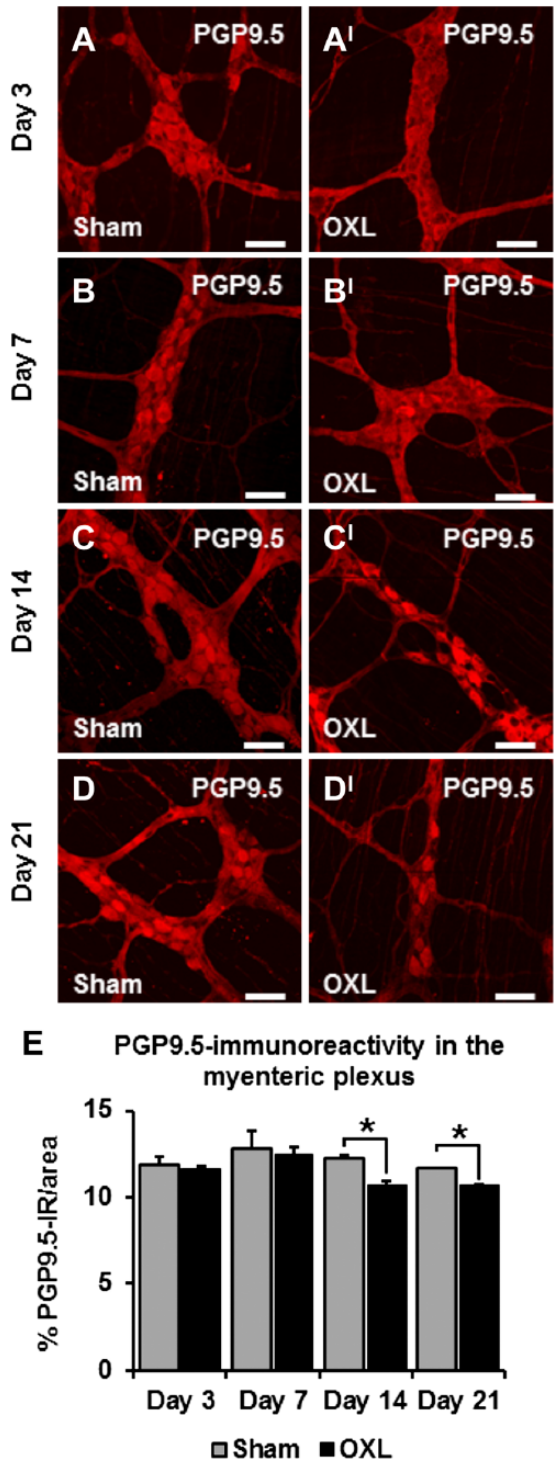

Figure 5. The effect of in vivo oxaliplatin treatment on protein gene product 9.5-IR (PGP9.5-IR) neurons in the myenteric plexus. PGP9.5 immunoreactivity in longitudinal muscle-myenteric plexus (LMMP) ileum preparations 3, 7, 14, and 21 days after commencement of oxaliplatin treatment (A–D^{I}). Scale bars = 50 µm. Quantitative analyses measuring the density of PGP9.5-IR neurons per 2 mm^2 area (E). *n*=3 mice/group/time point. Abbreviation: OXL = oxaliplatin. *p<0.05.

Effects of Oxaliplatin Treatment on the Myenteric Neurons of the Ileum

Myenteric neurons in the mouse ileum were examined following repeated oxaliplatin treatment with an antibody to the neuronal marker PGP9.5 that labeled neuronal cell bodies and processes (Fig. 5). No differences were found in the density of PGP9.5-IR per 2 mm^2 area in the ileum at 3 and 7 days after commencement of oxaliplatin treatment (day 3: sham: 11.9 ± 0.4%, oxaliplatin: 11.6 ± 0.1%; day 7: sham: 12.9 ± 1.0%, oxaliplatin: 12.5 ± 0.4%; *n*=3 mice/group/time point; Figs. 5A and B^{I}, E). However, quantification of the density of PGP9.5-IR in the myenteric plexus of the ileum after 14 days demonstrated loss of myenteric neurons in tissues from oxaliplatin-treated mice (sham: 12.2 ± 0.2%, oxaliplatin: 10.7 ± 0.2%, p<0.05; *n*=3 mice/group/time point; Figs. 5C–C^{I}). Similarly, reduction in the density of PGP9.5-IR was observed at 21 days after the commencement of oxaliplatin treatment (sham: 11.7 ± 0.01%, oxaliplatin: 10.7 ± 0.1%, p<0.05; *n*=3 mice/group/time point; Figs. 5D and E).

Effects of Oxaliplatin Treatment on EGCs and Neurons in the SMP

The effects of repeated oxaliplatin treatment on EGCs were assessed in the SMP of the mouse ileum at day 14 (Figs. 6A–D^{II}). A significant decrease in the density of submucosal GFAP-IR was revealed in whole mount tissues from oxaliplatin-treated mice (1.1 ± 0.04%) when compared with tissues from sham-treated mice (1.7 ± 0.1%, *n*=3 mice/group, p<0.01; Figs. 6A, B, and E). There were no changes to the density of s100β-IR labeling in the submucosal ganglia of the ileum from oxaliplatin-treated mice (2.7 ± 0.1%) when compared with sham-treated animals (2.5 ± 0.1%, *n*=3 mice/group; Figs. 6C, D, and F). Quantification of β-Tubulin (III)-IR in submucosal preparations revealed a decrease in neuronal cell bodies and fibers in the oxaliplatin group at day 14 (oxaliplatin: 2.2 ± 0.1%, sham: 2.8 ± 0.1%, *n*=3 animals/group, p<0.05; Figs. 6A^{I}, D^{I}, and G).

Effects of Oxaliplatin Treatment on EGCs in Cross-Sections of the Ileum

GFAP and s100β immunoreactivity was quantified in cross-sections (per 2 mm^2 area) of the ileum 14 days after the commencement of oxaliplatin treatment (Figs. 7A and B^{II}). Consistent with results observed in the myenteric and submucosal plexi,

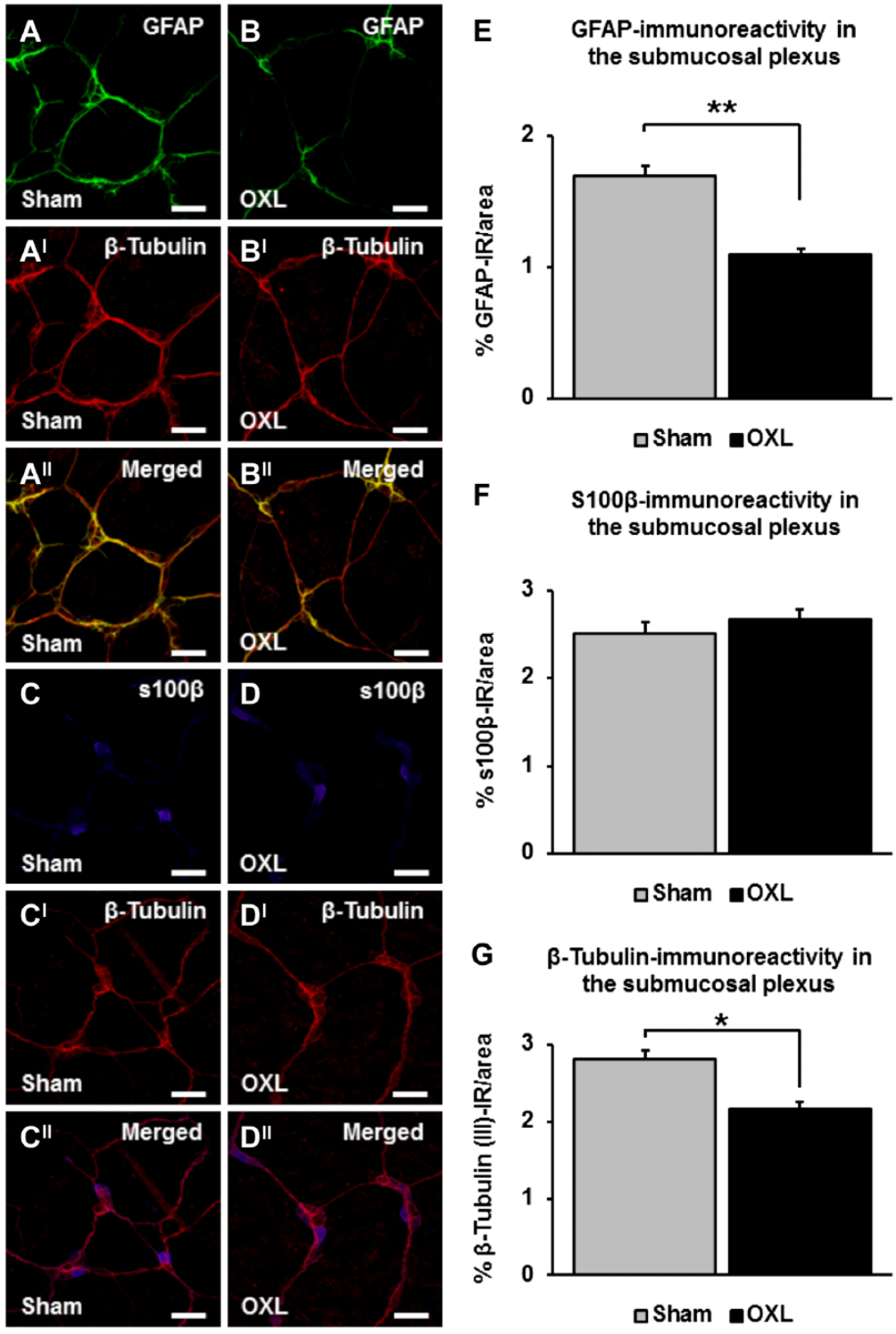

Figure 6. The effects of long-term oxaliplatin treatment on glial fibrillary acidic protein (GFAP) and s100β-immunoreactive (IR) enteric glial cells (EGCs) in the submucosal plexus (SMP). GFAP-IR EGCs (A–B), s100β-IR EGCs (C–D), and β-Tubulin-IR neurons and fibers (A^{I}–D^{I}) in the SMP of the ileum 14 days after the commencement of oxaliplatin treatment. Merged images of submucosal neurons and EGCs (A^{II}–D^{II}). Scale bars = 50 μm. Quantitative analyses of the density of GFAP immunoreactivity per 2 mm^2 area (E), s100β immunoreactivity per 2 mm^2 area (F), and β-Tubulin (III) immunoreactivity per 2 mm^2 area (G) in submucosal preparations. *n*=3 mice/group. Abbreviation: OXL = oxaliplatin. *p<0.05, **p<0.01.

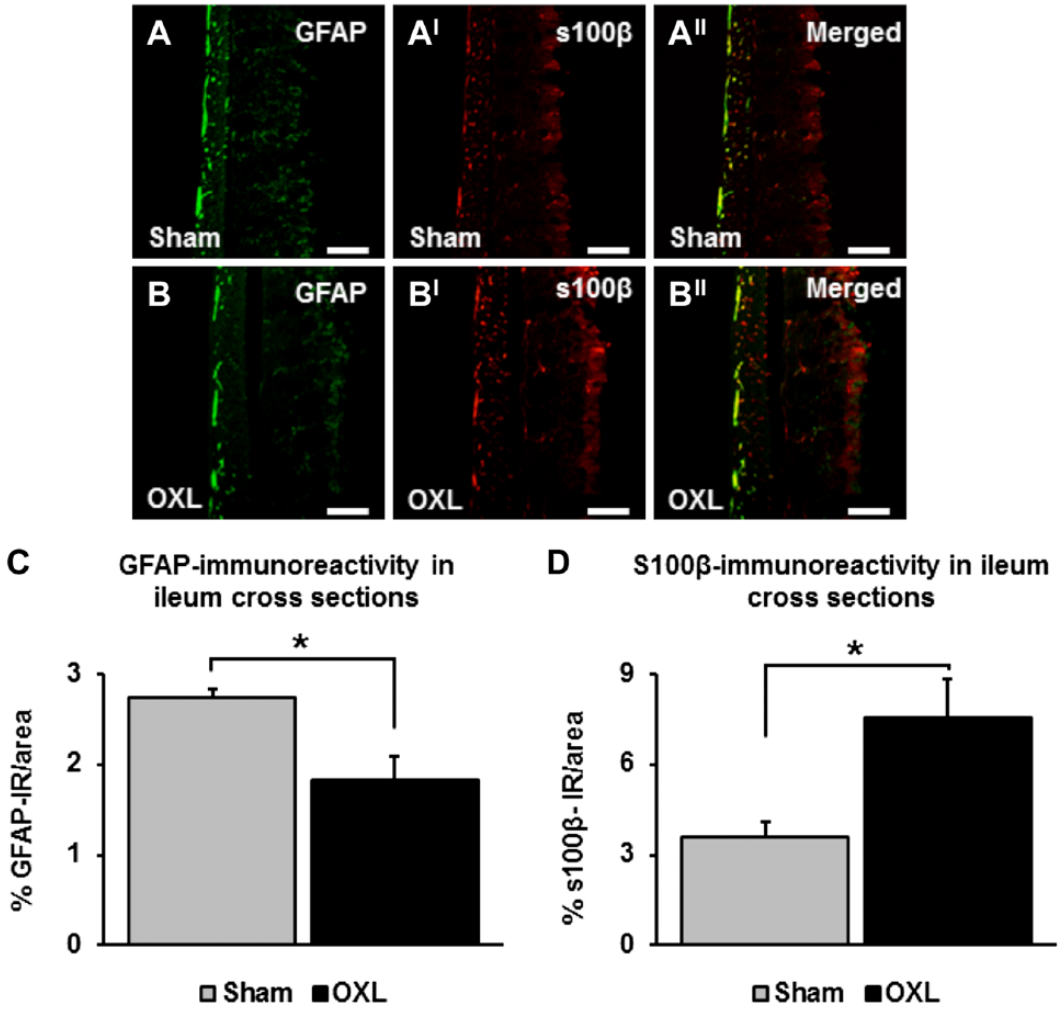

Figure 7. The effects of long-term oxaliplatin treatment on glial fibrillary acidic protein (GFAP) and s100β-IR enteric glial cells (EGCs) in cross-sections of the ileum. GFAP-IR (A–B) and s100β-IR (A^{I}–B^{I}) EGCs in cross-sections of the ileum 14 days after the commencement of oxaliplatin treatment. Merged images (A^{II}–B^{II}). Scale bars = 100 μm. The density of GFAP (C) and s100β (D) immunoreactivity measured in cross-sections of the ileum. *n*=3 mice/group. Abbreviation: OXL = oxaliplatin. *p<0.05.

GFAP immunoreactivity decreased in cross-sections of the ileum from oxaliplatin-treated mice (1.8 ± 0.3%) when compared with sham-treated mice (2.7 ± 0.1%, *n*=3 animals/group, p<0.05; Fig. 7C). s100β immunoreactivity was increased in sections from the oxaliplatin-treated group at 14 days (oxaliplatin: 7.6 ± 1.2%, sham: 3.6 ± 0.5%, *n*=3 animals/group, p<0.05; Fig. 7D).

Effects of Oxaliplatin Treatment on the Level of GFAP and s100β-Protein Expression

Western blotting was performed on lysates made from the smooth muscle and enteric ganglia layers. Antiserum against GFAP protein (a single band at approximately 48 kDa) revealed a significant reduction in GFAP expression from the oxaliplatin-treated mice ($0.6 \pm 0.2 \times 10^6$) when compared with protein levels in sham-treated animals ($2.4 \pm 0.3 \times 10^6$, *n*=3 animals/group, p<0.01; Figs. 8A and B). However, assessment of ileum s100β-protein levels (a single band at approximately 11 kDa) revealed increase in s100β expression in tissues from oxaliplatin-treated animals (oxaliplatin: $3.8 \pm 1.1 \times 10^6$, *n*=7, p<0.05; sham: $0.6 \pm 0.1 \times 10^6$, *n*=5, Figs. 8A and C). Western blotting of β-Tubulin (III) protein (a single band at approximately 55 kDa) levels demonstrated a reduced expression in tissues from oxaliplatin-treated mice (6.6 ± 0.5, p<0.05) when compared with tissues from sham-treated animals (10.0 ± 1.0, *n*=3 mice/group; Figs. 8A and D).

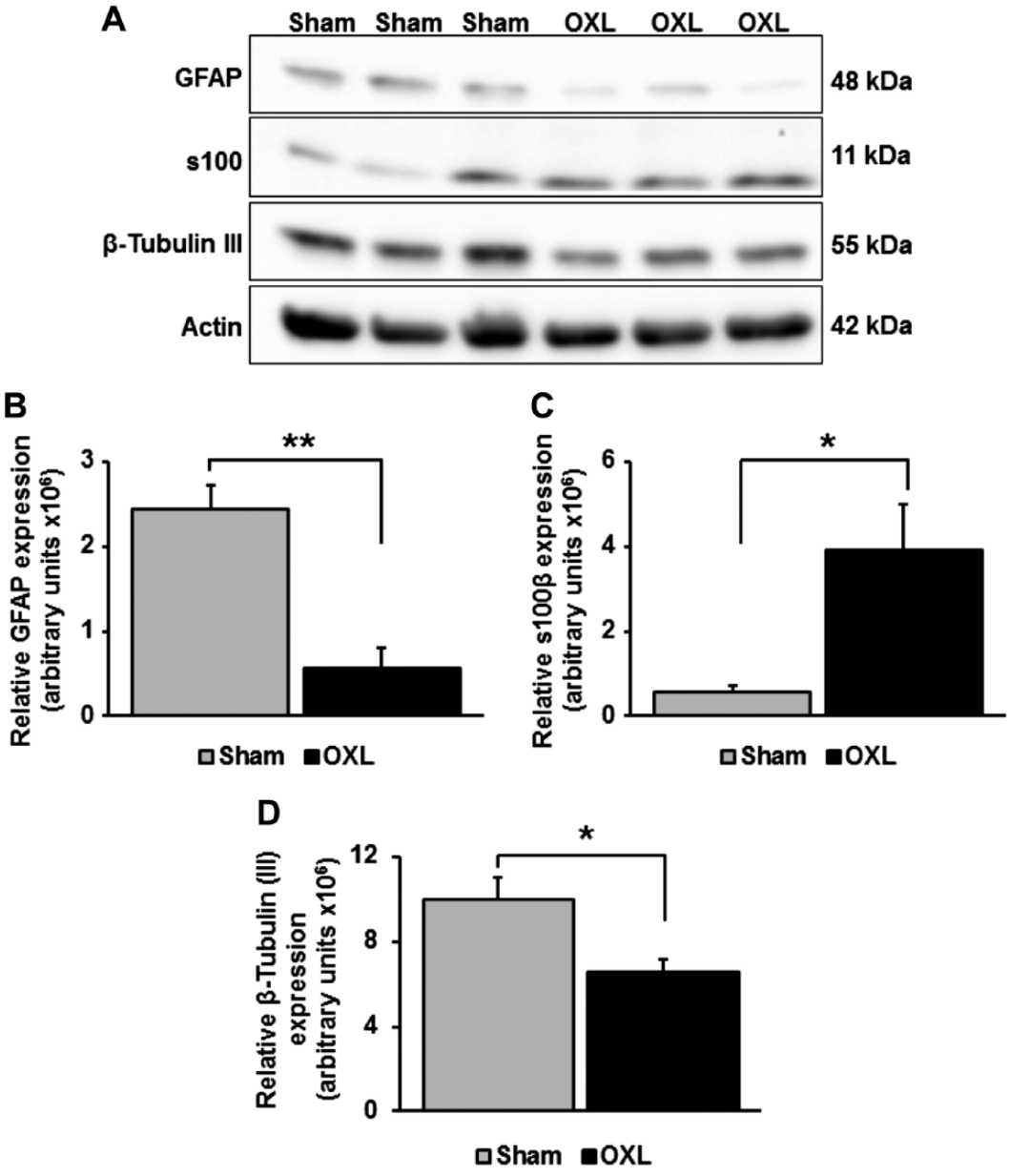

Figure 8. The effects of long-term oxaliplatin treatment on glial fibrillary acidic protein (GFAP), s100β, and β-Tubulin (III) protein expression in the ileum. A representative result of Western blot analysis for GFAP, s100β, and β-Tubulin (III) protein expression in the myenteric ganglia/smooth muscle preparations (A). Actin was used as a loading control. Relative expression of GFAP (B), s100β (C), and β-Tubulin (III) (D) proteins in the ileum at 14 days after the commencement of oxaliplatin treatment. *n*=3–7 mice/group. Abbreviation: OXL = oxaliplatin. **p*<0.05, ***p*<0.01.

Discussion

The objective of this study was to investigate the effects of repeated in vivo oxaliplatin treatment on the EGCs and neurons in the mouse ileum. The present study showed that (1) short-term oxaliplatin treatment did not affect the density of EGCs or neurons in the myenteric plexus of the ileum, (2) long-term oxaliplatin treatment (14–21 days) induced decrease in the density of GFAP immunoreactivity in both myenteric and submucosal ganglia and in cross-sections and increase in s100β immunoreactivity in myenteric ganglia and mucosa, (3) long-term oxaliplatin treatment instigated loss of myenteric and submucosal neurons in the ileum, and (4) changes in expression of GFAP and s100β proteins following long-term oxaliplatin treatment were confirmed by Western blot analyses performed in the myenteric ganglia/smooth muscle preparations at day 14.

Diverse populations of glial cells in the gut IR for s100β and GFAP reside within myenteric and submucosal ganglia, within interganglionic nerve fiber tracts, beneath mucosal epithelial cells, and between smooth muscle cells.[23,38] Mature EGCs are rich in the intermediate filament protein GFAP.[39,40] Although GFAP does not consistently differentiate between intrinsic and extrinsic glia, it is recognized as a specific glial cell marker to identify GFAP-positive EGCs[16] and to distinguish any variances in EGC morphology.[41] A small, diffusible neurotrophin s100β is located in the cytoplasm or nucleus of cells in both nervous system and non-nervous system tissues.[28] The gut s100β protein, a small signaling diffusible Ca^{2+}/Zn^{2+}-binding protein, is specifically expressed by EGCs.[27,42] This protein regulates cytoskeletal structure and function and Ca^{2+} homeostasis in the cytoplasm of glial cells.[43] Thus, two antibodies, anti-GFAP and anti-s100β, were utilized in this study to identify EGCs at the levels of the myenteric and submucosal plexi, as well as across the entire ileum wall. In the mouse ileum, the submucosal ganglia when compared with the myenteric ganglia have much smaller number of glial cells.[44] Accordingly, the densities of both GFAP-IR and s100β-IR EGCs were different between the myenteric and submucosal plexi of the ileum from control mice observed in our study. Moreover, our results are consistent with previously reported differential expression of s100β and GFAP in the myenteric[38,45] and submucosal[45] plexi of the intestine from control mice and rats.

In the present study, long-term repeated oxaliplatin administration caused decrease in the expression of GFAP in the myenteric and submucosal plexi as well as in cross-sections of the ileum confirmed by Western blot analysis performed in the myenteric ganglia/smooth muscle preparations at day 14. GFAP expression is modulated by cell differentiation, inflammation, and injury,[40] indicating that the level of this intermediate filament protein matches with the functional state of EGC. Disruption of EGCs has been characterized by a decrease in GFAP expression both at the protein and mRNA level in a transgenic mouse model of EGC disruption.[46] Consistent with our results, decrease in GFAP expression has been observed in other pathological conditions. In vivo studies using type 1 diabetic mice have shown decreases in CNS[47] and colonic levels of GFAP.[48,49] In addition, the expression of GFAP has been reported to decrease in response to acute infection, neurodegeneration, and conditions such as Wernicke's encephalopathy, Down's syndrome, schizophrenia, bipolar disorder, and depression.[50] GFAP-null mice have delayed nerve regeneration following an injury.[51]

In our study, the density of s100β-IR EGCs was increased in the myenteric plexus (confirmed by IHC in whole mount preparations of myenteric ganglia and by Western Blot) and in mucosa (demonstrated by IHC in cross-sections). Elevated s100β expression has been previously associated with Alzheimer's disease and traumatic brain and spinal cord injury, where an increase in this protein is due to neuronal or glial cell insult.[52–54] Furthermore, increased s100β expression within the dorsal root ganglion (DRG) is also observed following sciatic nerve transection.[55] In the gut, aberrant expression of s100β protein participates in the onset and progression of inflammatory status, orchestrating a wide range of proinflammatory pathways that are directly involved in intestinal inflammation.[27,28,42] Previous studies have reported increases in EGC-derived s100β mRNA, protein expression, and secretion in the duodenum of patients with celiac disease and Crohn's disease, as well as in the rectal mucosa of ulcerative colitis patients.[27,42]

The differences in GFAP and s100β functions may explain the opposite effects of oxaliplatin treatment on the expression of these proteins observed in our study. GFAP is typically associated with regeneration, whereas s100β is linked to cell damage and apoptosis.[51,56] Decreased level of GFAP and increased level of s100β immunoreactivity within myenteric plexus and in the mucosa (subepithelial EGCs) observed in our study is indicative of cellular damage associated with oxaliplatin treatment. However, no changes in the levels of s100β immunoreactivity were observed in SMP following oxaliplatin treatment. It has been reported previously that submucosal and myenteric EGCs respond differently to damaging stimuli such as proinflammatory cytokines.[57] These results might reflect functional heterogeneity of EGCs and differences in their response to chemotherapy-induced intestinal damage.

A decrease in the population of EGCs colocalizing GFAP and s100β was observed in the myenteric plexus of oxaliplatin-treated mice. Whether the decrease in GFAP/s100β colocalization is due to phenotypic changes in EGCs or due to the loss of GFAP-IR EGC population, and increase in proliferation of s100β-IR EGC population, needs to be further determined.

Our results demonstrated that changes in GFAP and s100β expressions in oxaliplatin-treated animals correlated with decreased density of myenteric and submucosal neurons in the ileum after 14 days of repeated administration. This is consistent with previous reports on the reduction in the number of enteric neurons in the colon after administration of oxaliplatin in mice[34] and cisplatin in rats.[33] These changes in the ENS were associated with lack of weight gain, pica, and constipation that correlate with changes in gastrointestinal transit and colonic motility observed in oxaliplatin-treated mice.[8,34]

Some of these symptoms start soon after the first injection (e.g., pica, changes in gastrointestinal transit), while others have delayed onset (e.g., constipation observed at days 14 and 21 after the start of treatment). The early symptoms might be due to the mucosal damage associated with chemotherapy.[6,58] We have not observed obvious mucosal damage or macroscopic lesions in the ileum at the time points we studied. However, this cannot be excluded at the earlier time points (within hours of oxaliplatin administration) as in our previous studies, using a model of 2,4,6-trinitrobenzenesulfonic acid (TNBS)–induced ileitis, we have seen mucosal damage occurring within the first few hours and mucosal regeneration by day 3.[59,60] Early mucosal damage can lead to damage and death of enteric neurons leading to long-term gastrointestinal dysfunction.[60,61] However, direct oxaliplatin toxicity is another possible mechanism of the enteric neuronal and glial cell damage underlying long-term gastrointestinal symptoms.[11,12] The mechanisms underlying neuronal loss resulting from chemotherapy treatment have not been elucidated. However, the role of glial cells in chemotherapy-induced neurotoxicity has been implicated.[32] It has been reported that oxaliplatin-induced neuropathies show different characteristics of tissue injury with changes in the density of glial cells in the presence of limited alteration of cell morphology.[29] Cisplatin-induced toxicity to human and rat Schwann cells has been previously studied and it has been revealed that platinum-based agent can accumulate within glial cells.[62,63] Other studies have reported that DRG neurons undergo apoptosis following exposure to oxaliplatin.[64,65] Dense *vascularization* of the DRG neurons and glial cells makes them vulnerable to preferential accumulation and injury from chemotherapeutic agents.[66] Cisplatin and oxaliplatin accumulation in DRG neurons is correlated with increased platinum-DNA binding in and death of neurons.[64,67] Given that both glia and neurons within the nervous system are vulnerable to platinum accumulation and cell damage and death, this may also be the mechanism contributing to oxaliplatin-induced glial and neuronal toxicity within the ENS leading to gastrointestinal dysfunction.

In summary, repeated in vivo oxaliplatin administration induces aberrant effects on the EGCs that were most prominent at 14 days after commencement of treatment. The changes in expression of GFAP and s100β-IR EGCs observed in this study are associated with neuronal loss induced by oxaliplatin treatment, implicating the role of EGCs in oxaliplatin-induced enteric neurotoxicity and long-term gastrointestinal dysfunction.

Author Contributions

AMR performed experiments, analyzed data, and wrote the manuscript. VS and PVS performed experiments, analyzed data, and contributed to manuscript writing. AAR and RMM contributed to processing tissues for immunohistochemical and histological studies. KN developed the concept, edited manuscript, obtained funding, and supervised the study.

Competing Interests

The authors declared no potential conflicts of interest with respect to the research, authorship, and/or publication of this article.

Funding

The authors disclosed receipt of the following financial support for the research, authorship, and/or publication of this article: This study was supported by a Victoria University Research Support Grant.

Literature Cited

1. Golfinopoulos V, Salanti G, Pavlidis N, Ioannidis JP. Survival and disease-progression benefits with treatment regimens for advanced colorectal cancer: a meta-analysis. Lancet Oncol. 2007;8:898–911.
2. Capdevila J, Elez E, Peralta S, Macarulla T, Ramos FJ, Tabernero J. Oxaliplatin-based chemotherapy in the management of colorectal cancer. Exp Rev Anti-cancer Ther. 2008;8:1223–36.
3. Bhushan S, McLeod H, Walko CM. Role of pharmacogenetics as predictive biomarkers of response and/or toxicity in the treatment of colorectal cancer. Clin Colorectal Cancer. 2009;8:15–21.
4. Goldberg RM. Advances in the treatment of metastatic colorectal cancer. Oncologist. 2005;10:40–48.
5. Kiernan MC, Krishnan AV. The pathophysiology of oxaliplatin-induced neurotoxicity. Cur Med Chem. 2006;13:2901–7.
6. Di Fiore F, Van Cutsem E. Acute and long-term gastrointestinal consequences of chemotherapy. Best Prac Res Clin Gastroenterol. 2009;23:113–24.
7. Alcindor T, Beauger N. Oxaliplatin: a review in the era of molecularly targeted therapy. Curr Oncol. 2011;18:18–25.
8. McQuade RM, Bornstein JC, Nurgali K. Anti-colorectal cancer chemotherapy-induced diarrhoea: current treatments and side-effects. Int J Clin Med. 2014;5:393–406.
9. Hartmann JT, Lipp HP. Toxicity of platinum compounds. Exp Opin Pharmacother. 2003;4:889–901.
10. Weickhardt A, Wells K, Messersmith W. Oxaliplatin-induced neuropathy in colorectal cancer. J Oncol. 2011;2011:1–7.
11. Stojanovska V, Sakkal S, Nurgali K. Platinum-based chemotherapy: gastrointestinal immunomodulation and enteric nervous system toxicity. Am J Physiol. 2015;308:G223–32.
12. Pini A, Garella R, Idrizaj E, Calosi L, Baccari MC, Vannucchi MG. Glucagon-like peptide 2 counteracts

the mucosal damage and the neuropathy induced by chronic treatment with cisplatin in the mouse gastric fundus. Neurogastroenterol Motil. 2016;28:206–16.
13. Furness JB. The enteric nervous system and neurogastroenterology. Nat Rev Gastroenterol Hepatol. 2012;9:286–4.
14. Cabarrocas J, Savidge TC, Liblau RS. Role of enteric glial cells in inflammatory bowel disease. Glia. 2003;41:81–93.
15. Ruhl A, Nasser Y, Sharkey KA. Enteric glia. Neurogastroenterol Motil. 2004;16:44–49.
16. Ruhl A. Glial cells in the gut. Neurogastroenterol Motil. 2005;17:777–90.
17. Von Boyen G, Steinkamp M. The enteric glia and neurotrophic factors. Gastroenterology. 2006;44:985–90.
18. Von Boyen G, Steinkamp M, Geerling I, Reinshagen M, Schafer KH, Adler G, Kirsch J. Proinflammatory cytokines induce neurotrophic factor expression in enteric glia: a key to the regulation of epithelial apoptosis in Crohn's disease. Inflamm Bowel Dis. 2006;12:346–54.
19. Neunlist M, Rolli-Derkinderen M, Latorre R, Van Landeghem L, Coron E, Derkinderen P, De Giorgio R. Enteric glial cells: recent developments and future directions. Gastroenterology. 2014;147:1230–7.
20. Vasina V, Barbara G, Talamonti L, Stanghellini B, Corinaldesi R, Tonini M, De Ponti F, De Giorgio R. Enteric neuroplasticity evoked by inflammation. Auton Neurosci. 2006;126–127:264–72.
21. Bassotti G, Villanacci V, Cathomas G, Maurer CA, Fisogni S, Cadei M, Baron L, Morelli A, Valloncini E, Salerni B. Enteric neuropathology of the terminal ileum in patients with intractable slow-transit constipation. Hum Pathol. 2006;37:1252–8.
22. Bassotti G, Villanacci V, Fisogni S, Rossi E, Baronio P, Clerici C, Maurer CA, Cathomas G, Antonelli E. Enteric glial cells and their role in gastrointestinal motor abnormalities: introducing the neuro-gliopathies. World J Gastroenterol. 2007;13:4035–41.
23. Gulbransen BD, Sharkey KA. Novel functional roles for enteric glia in the gastrointestinal tract. Nat Rev Gastroenterol Hepatol. 2012;9:625–32.
24. McClain JL, Grubišić V, Fried D, Gomez-Suarez RA, Leinninger GM, Sévigny J, Parpura V, Gulbransen BD. Ca^{2+} responses in enteric glia are mediated by connexin-43 hemichannels and modulate colonic transit in mice. Gastroenterology. 2014;146:497–507.
25. Iantorno G, Bassotti G, Kogan Z, Lumi CM, Cabanne AM, Fisogni S, Varrica LM, Bilder CR, Munoz JP, Liserre B, Morelli A, Villanacci V. The enteric nervous system in chagasic and idiopathic megacolon. Am J Surg Pathol. 2007;31:460–68.
26. Thacker M, Rivera LR, Cho H, Furness JB. The relationship between glial distortion and neuronal changes following intestinal ischemia and reperfusion. Neurogastroenterol Motil. 2011;23:500–509.
27. Esposito G, Cirillo C, Sarnelli G, De Filippis D, D'Armiento FP, Rocco A, Nardone G, Petruzzelli R, Grosso M, Izzo P, Iuvone T, Cuomo R. Enteric glial-derived s100β protein stimulates nitric oxide production in celiac disease. Gastroenterology. 2007;133:918–25.
28. Cirillo C, Sarnelli G, Esposito G, Turco F, Steardo L, Cuomo R. S100β protein in the gut: the evidence for enteroglial-sustained intestinal inflammation. World J Gastroenterol. 2011;17:1261–6.
29. Di Cesare Mannelli L, Pacini A, Bonaccini L, Zanardelli M, Mello T, Ghelardini C. Morphologic features and glial activation in rat oxaliplatin-dependent neuropathic pain. J Pain. 2013;14:1585–600.
30. Scholz J, Woolf CJ. The neuropathic pain triad: neurons, immune cells and glia. Nat Neurosci. 2007;10:1361–8.
31. Gao YJ, Ji RR. Targeting astrocyte signalling for chronic pain. Neurotherapeutics. 2010;7:482–93.
32. Di Cesare Mannelli L, Pacini A, Micheli L, Tani A, Zanardelli M, Ghelardini C. Glial role in oxaliplatin-induced neuropathic pain. Exp Neurol. 2014;261:22–33.
33. Vera G, Castillo M, Cabezos PA, Chiarlone A, Martín MI, Gori A, Pasquinelli G, Barbara G, Stanghellini V, Corinaldesi R, De Giorgio R, Abalo R. Enteric neuropathy evoked by repeated cisplatin in the rat. Neurogastroenterol Motil. 2011;23:370–8.
34. Wafai L, Taher M, Jovanovska V, Bornstein JC, Dass CR, Nurgali K. Effects of oxaliplatin on mouse myenteric neurons and colonic motility. Front Neurosci. 2013;7:30.
35. Reagan-Shaw S, Nihal M, Ahmad N. Dose translation from animal to human studies revisited. FASEB J. 2008;22:659–61.
36. Renn CL, Carozzi VA, Rhee P, Gallop D, Dorsey SG, Cavaletti G. Multimodal assessment of painful peripheral neuropathy induced by chronic oxaliplatin-based chemotherapy in mice. Mol Pain. 2011;7:29.
37. Rivero-Gutiérrez B, Anzola A, Martinez-Augustin O, Sanchez de Medina F. Stain-free detection as loading control alternative to Ponceau and housekeeping protein immunodetection in Western blotting. Analyt Biochem. 2014;467:1–3.
38. Boesmans W, Lasrado R, Vanden Berghe P, Pachnis V. Heterogeneity and phenotypic plasticity of glial cells in the mammalian enteric nervous system. Glia. 2015;63:229–41.
39. Jessen KR, Mirsky R. Glial cells in the enteric nervous system contain glial fibrillary acidic protein. Nature. 1980;286:736–7.
40. Eng LF, Ghirnikar RS, Lee YL. Glial fibrillary acidic protein: GFAP-thirty-one years (1969-2000). Neurochem Res. 2000;25:1439–51.
41. Ruhl A, Franzke S, Stremmel W. IL-1beta and IL-10 have dual effects on enteric glial cell proliferation. Neurogastroenterol Motil. 2001;13:89–94.
42. Cirillo C, Sarnelli G, Esposito G, Grosso M, Petruzzelli R, Izzo P, Cal G, D'Armiento FP, Rocco A, Nardone G, Iuvone T, Steardo L, Cuomo R. Increased mucosal nitric oxide production in ulcerative colitis is mediated in part by the enteroglial-derived S100B protein. Neurogastroenterol Motil. 2009;21:1209–12.
43. Heizmann CW. The multifunctional S100 protein family. Methods Mol Biol. 2002;172:69–80.

44. Gabella G, Trigg P. Size of neurons and glial cells in the enteric ganglia of mice, guinea-pigs, rabbits and sheep. J Neurocytol. 1984;13:49–71.
45. Rosenbaum C, Schick MA, Wollborn J, Heider A, Scholz C-J, Cecil A, Niesler B, Hirrlinger J, Walles H, Metzge M. Activation of myenteric glia during acute inflammation *in vitro* and *in vivo*. PLoS ONE. 2016;11:e0151335.
46. Aube AC, Cabarrocas J, Bauer J, Philippe D, Aubert P, Doulay F, Liblau R, Galmiche JP, Neunlist M. Changes in enteric neuron phenotype and intestinal functions in a transgenic mouse model of enteric glia disruption. Gut. 2006;55:630–37.
47. Coleman E, Judd R, Hoe L, Dennis J, Posner P. Effects of diabetes mellitus on astrocyte GFAP and glutamate transporters in the CNS. Glia. 2004;48:166–78.
48. Liu W, Yue W, Wu R. Effects of diabetes on expression of glial fibrillary acidic protein and neurotrophins in rat colon. Auton Neurosci. 2010;154:79–83.
49. Stenkamp-Strahm C, Patterson S, Boren J, Gericke M, Balemba O. High-fat diet and age-dependent effects on enteric glial cell populations of mouse small intestine. Auton Neurosci. 2013;177:199–210.
50. Johnston-Wilson NL, Sims CD, Hofmann JP, Anderson L, Shore AD, Torrey EF, Yolken RH. Disease-specific alterations in frontal cortex brain proteins in schizophrenia, bipolar disorder, and major depressive disorder. Mol Psychiatry. 2000;5:142–9.
51. Triolo D, Dina G, Lorenzetti I, Malaguti M, Morana P, Del Carro U, Comi G, Messing A, Quattrini A, Previtali SC. Loss of glial fibrillary acidic protein (GFAP) impairs Schwann cell proliferation and delays nerve regeneration after damage. J Cell Sci. 2006;1:3981–93.
52. Marshak DR, Pesce SA, Stanley LC, Griffin WS. Increased S100 beta neurotrophic activity in Alzheimer's disease temporal lobe. Neurobiol Aging. 1992;13:1–7.
53. Cao F, Yang XF, Liu WG, Hu WW, Li G, Zheng XJ, Shen F, Zhao Xq, Lv ST. Elevation of neuron-specific enolase and S-100beta protein level in experimental acute spinal cord injury. J Clin Neurosci. 2008;15:541–4.
54. Kwon BK, Stammers AM, Belanger LM, Bernardo A, Chan D, Bishop CM, Slobogean GP, Zhang H, Umedaly H, Giffin M, Street J, Boyd MC, Paquette SJ, Fisher CG, Dvorak MF. Cerebrospinal fluid inflammatory cytokines and biomarkers of injury severity in acute human spinal cord injury. J Neurotrauma. 2010;27:669–82.
55. Huang YL, Ding M, Hansson HA. Dorsal root ganglion nerve cells transiently express increased immunoreactivity of the calcium-binding protein S-100β after sciatic nerve transection. Brain Res. 1998;785:351–4.
56. Hu J, Ferreira A, Van Eldik LJ. S100beta induces neuronal cell death through nitric oxide release from astrocytes. J Neurochem. 1997;69:2294–301.
57. Tjwa ET, Bradley JM, Keenan CM, Kroese AB, Sharkey KA. Interleukin-1beta activates specific populations of enteric neurons and enteric glia in the guinea pig ileum and colon. Am J Physiol Gastrointest Liver Physiol. 2003;285:G1268–76.
58. Keefe DM. Mucositis management in patients with cancer. Support Cancer Ther. 2006;3:154–7.
59. Pontell L, Castelucci P, Bagyanszki M, Jovic T, Thacker M, Nurgali K, Bron R, Furness JB. Structural changes in the epithelium of the small intestine and immune cell infiltration of enteric ganglia following acute mucosal damage and local inflammation. Virchows Archiv. 2009;455:55–65.
60. Nurgali K, Qu Z, Hunne B, Thacker M, Pontell L, Furness JB. Morphological and functional changes in the guinea-pig neurons projecting to the ileal mucosa at early stages after inflammatory damage. J Physiol. 2011;589:325–39.
61. Nurgali K, Nguyen TV, Matsuyama H, Thacker M, Robbins HL, Furness JB. Phenotypic changes of morphologically identified myenteric neurons following intestinal inflammation. J Physiol. 2007;583:593–609.
62. Sugimoto T, Takeyama A, Fujita M, Ichikawa H, Takano-Yamamoto T. Peripheral neuroglial death induced by cisplatin administration in newborn rats. Neuroreport. 2001;12:137–40.
63. Jirsova K, Mandys V, Gispen WH, Bär PR. Cisplatin-induced apoptosis in cultures of human Schwann cells. Neurosci Lett. 2006;392:22–26.
64. Ta LE, Espeset L, Podratz J, Windebank AJ. Neurotoxicity of oxaliplatin and cisplatin for dorsal root ganglion neurons correlates with platinum–DNA binding. Neurotoxicology. 2006;27:992–1002.
65. Scuteri A, Galimberti A, Maggioni D, Ravasi M, Pasini S, Nicolini G, Bossi M, Miloso M, Cavaletti G, Tredici G. Role of MAPKs in platinum-induced neuronal apoptosis. Neurotoxicology. 2009;30:312–9.
66. Jimenez-Andrade J, Herrera M, Ghilardi J, Vardanyan M, Melemedjian O, Mantyh P. Vascularization of the dorsal root ganglia and peripheral nerve of the mouse: implications for chemical-induced peripheral sensory neuropathies. Mol Pain. 2008;4:10.
67. McDonald ES, Randon KR, Knight A, Windebank AJ. Cisplatin preferentially binds to DNA in dorsal root ganglion neurons in vitro and in vivo: a potential mechanism for neurotoxicity. Neurobiol Dis. 2005;18:305–13.